Structural, energetic and electronic properties of (100) surfaces for alkaline earth metal oxides as calculated with hybrid density functional theory

Andrew J. Logsdail [a], David Mora-Fonz [a], David O. Scanlon [a,b], C. Richard A. Catlow [a], Alexey A. Sokol [a]

[a] *University College London, Kathleen Lonsdale Materials Chemistry, Department of Chemistry, 20 Gordon St., London WC1H 0AJ, United Kingdom*
[b] *Diamond Light Source Ltd., Diamond House, Harwell Science and Innovation Campus, Didcot, Oxfordshire OX11 0DE, United Kingdom*

A B S T R A C T

We perform a systematic investigation of (100) surfaces for rocksalt-structured group 2 metal oxides, namely MgO, CaO, SrO and BaO, using GGA and Hybrid-DFT exchange-correlation functionals. We examine the structural, energetic and electronic properties of the surfaces, with a specific focus on the surface ionisation potential and band bending; the latter of which we quantify by examining the density of states as a function of depth from the system surface. We report structural and energetic results in-line with previous experimental work when we use the Hybrid-DFT method, and for the electronic structure we find inequivalent band bending for the valence and conduction bands, which results in reduced ionisation potentials and the closure of the band gap at the surface when compared to bulk systems. We also report downward bending of the conduction band for MgO that brings it below the vacuum potential, unlike previous theoretical investigations, and thus indicates an origin of the positive electron affinity found in the experiment.

1. Introduction

Metal oxides are of technological importance due to their applications in fields such as heterogeneous catalysis and microelectronics [1–5], where surface stability is a desirable material characteristic [5,6]. For alkaline metal oxides that form in a rocksalt (NaCl) crystal structure, the (100) surface is particularly well studied owing to its stability and ease of experimental preparation [5,7,8]. A detailed understanding of the surface properties can be used to explain observed phenomena such as their differing catalytic activities: for instance, Liu et al. analysed the reaction of H_2O with MgO and CaO (100) surfaces, finding that the latter formed a surface hydroxide at significantly lower pressures [9,10]. It was suggested that dissociation of H_2O over MgO occurs only at surface defects [11] and subsequent theoretical calculations confirm this, with preference towards corner (3-coordinate Mg) and edge (4-coordinate Mg) sites [12–15]; more recent results suggest that the reactivity found over CaO would also occur for BaO [16,17]. CaO and SrO are also known to be better catalysts for the Tishchenko reaction: the dimerisation of aldehydes to form esters [18,19]. This

superiority may be related to the basicity of the lattice oxygens, as suggested from calculations for the etherification of glycerol where the reactivity is ordered BaO > SrO > CaO > MgO [20,21].

Creating a surface on a material results in an inherent stress, due to the undercoordination of surface atoms. This stress is typically relieved by structural relaxations and, in more complicated cases, atomic rearrangement [3,22–25]. Surface relaxation mechanisms have been proposed for ionic systems, with most models describing the relaxation in terms of the electrostatic interactions and short-range repulsion between ions [3,22]. In particular, the relative shift of surface cations and anions normal to the surface, i.e. surface rumpling, is suggested as being linked to the differences in the size and polarisability for the species, though the second neighbour interactions could also be important [3,26]. These structural changes, along with the "dangling-bonds" of the surface atoms, can lead to novel surface-specific electronic properties, such as band bending [6,27]. However, generally such changes for rocksalt oxides, like MgO, are small due to the maintenance of 5-fold coordination by the surface atoms and the relatively low levels of rumpling that occurs, though the introduction of defects is understood to alter this equilibrium significantly [28–30].

Table 1 presents previous experimental data for MgO surface rumpling (d_{rum}), which is the difference in the surface protrusion between

Table 1
Comparison of experimental (exp.) and theoretical rumpling (d_{rum}) and relaxation (d_{rel}) for (100) surfaces of MgO, along with surface energies (γ_{surf}). Method acronyms are as stated in the text; the -SIC appenditure on to LDA stands for "self-interaction correction", as applied in the specific calculation. The exchange-correlation functional is given in parentheses for theoretical results.

	Method	[Ref]	d_{rum} (%)	d_{rel} (%)	γ_{surf} (J/m^2)
Exp.:	LEED	[31]	–	-0.3 ± 1.6	–
	LEED	[32]	0	0–2.5	–
	LEED	[33]	2 ± 2	0 ± 0.75	–
	LEED	[34]	5 ± 2.5	1 ± 2	–
	LEED	[35]	3.3 ± 1.5	-0.2 ± 0.7	–
	CAICISS	[36]	0.3 ± 0.9	-15 ± 3	–
	MEIS	[37]	0.5 ± 1.0	-1.0 ± 1.0	–
	GIXS	[38]	1.07 ± 0.5	-0.56 ± 0.35	–
	FAD	[39]	0.03 ± 0.03	–	–
		[46]	–	–	1.04
Theory:	LDA (VWN)	[23]	1.87	0.22	1.18
	LDA (PZ81)	[41]	1.8	-0.2	1.14
	LDA (LSDA)	[42]	0.95	-1.4	
	LDA-SIC (PZ81)	[43]	2.0	0.1	1.29
	GGA (PBE)	[23]	2.40	-0.43	0.90
	GGA (PBE)	[41]	2.2	-0.2	1.02
	GGA (PW91)	[44]	2.27	0.00	0.90
	GGA (PW91)	[45]	2.2	0.0	0.83
	GGA (PBE-D)	[39]	0.06	–	–
	Hybrid (B3LYP)	[47]	1.5	-2.9	–

cation and anion species relative to the bulk interlayer separation; Table 1 also gives the surface relaxation (d_{rel}), which is the separation of the surface layer from the next underlying layer when compared to the bulk lattice constant. These are illustrated in Fig. 1, and defined as [23]:

$$d_{rum} = \frac{Z_a^{(1)} - Z_c^{(1)}}{Z_0}, \tag{1}$$

$$d_{rel} = \frac{\left[\left(Z_a^{(1)} + Z_c^{(1)}\right)/2 - \left(Z_a^{(2)} + Z_c^{(2)}\right)/2\right]}{Z_0} - 1, \tag{2}$$

where the surface normal is chosen to align with the Z-Cartesian axis, and Z_a and Z_c are used to identify the Z-coordinate of the anion and cation species, respectively, and Z_0 is the bulk interlayer distance ($= a_0/2$). The superscript notations $^{(1)}$ and $^{(2)}$ denote the surface and first subsurface layer respectively. A positive value of d_{rum} indicates that the anions protrude from the surface, farther than the cations; and a negative sign implies the inverse. For d_{rel}, a positive sign implies expansion between the surface layers, whilst a negative sign implies contraction.

Experimental measurements have mostly used low-energy electron diffraction (LEED), with a notable scatter in results such that d_{rel} could be interpreted as positive or negative [31–35]. d_{rum}, however, is

Fig. 1. Schematic representation of anions (red) and cations (blue) in a slab system, and the variables then used in the calculation of d_{rum} and d_{rel}. $Z_a^{(1)}$ and $Z_c^{(1)}$ are as defined in Eq. (1), whilst $\Delta Z^{(12)}$ is the inter-layer distance between the average position of layers $^{(1)}$ and $^{(2)}$, $[(Z_a^{(1)} + Z_c^{(1)})/2 - (Z_a^{(2)} + Z_c^{(2)})/2]$, as included in the numerator of Eq. (2). a_0 is the bulk lattice constant, and Z_0 ($= a_0/2$) is the bulk nearest neighbour distance.

unanimously positive with a range of 0 to 5%, indicating that the O^{2-} anions protrude farther from the surface than the Mg^{2+} cations, consistent with measurements using coaxial impact collision ion scattering spectroscopy (CAICISS) [36], medium energy ion scattering (MEIS) [37], grazing incidence X-ray scattering (GIXS) [38], and fast atom diffraction (FAD) [39]; the latter two methods in particular report improvements in accuracy, and reduced error bars. Complementary to these experiments have been a range of computational simulations, ranging from molecular mechanics based forcefield calculations [40], to higher-level Hartree-Fock (HF) calculations [28]. We have limited our literature data selection (Table 1) to density functional theory (DFT) calculations as we are specifically interested in these results in the context of our work; d_{rum} is positive in all cases, matching the experimental observations, but the results acquired using the local-density approximation (LDA) [23,41–43] are in general smaller than those obtained using the generalised-gradient approximation (GGA) [23,41,44, 45]. Contrastingly, d_{rel} varies between -1.4 (-0.43) and 0.22 (0.1) % for the LDA (GGA) calculations; for the Hybrid-DFT a significantly lower result of -2.9% is reported. Finally, we also give the surface energy (γ_{surf}), which for the reported calculations illustrates that the LDA (1.14–1.29 J/m^2, [23,41,43]) and GGA (0.83–1.02 J/m^2, [23,41,44,45]) methods slightly overestimate and underestimate, respectively, the energy required to create a (100) MgO surface when compared to the experimental measurement of 1.04 J/m^2, [46].

We summarise the available literature reports in Table 2 for other rocksalt structured metal oxides formed from the alkaline earth metals. The experimental literature for CaO is limited to a LEED experiment by Prutton et al. [48], though there are many DFT calculations [23,41, 43–45]: for these, d_{rum} is between -1.31 to -0.2%, which is the opposite sign to experiment in all cases (2%), whereas d_{rel} has the same sign though smaller in the experiment (-1%) than DFT (-1.12 to -2.7%). Comparing the LDA and GGA calculations, there are similar trends as for the MgO calculations: the LDA gives lower values of d_{rum} and d_{rel} compared to the GGA. However, these trends are not consistent for SrO and BaO, where the LDA and GGA results are similar. γ_{surf}, on the other hand, is consistently higher for the LDA by ~0.3 J/m^2 for CaO, SrO and BaO. In general all previous DFT calculations found that rumpling of the (100) surface becomes increasingly negative as one descends group 2 of the periodic table.

The structural and energetic changes at a surface are driven largely by the underlying electrostatic potential, which depends on factors such as the undercoordination of surface atoms and the varying polarisability of the respective constituent elements. The energy levels of electrons are also determined by the electrostatic potential [49], and typically one finds that the energy levels, particularly of the valence electrons, vary depending on the nature of a material. For an n-type material, such as ZnO, the electrostatic potential of e.g. an O^{2-} species generally decreases at a nonpolar surface, thus the energy of valence electrons rises, reducing the number of electrons occupying this spatial region [50,51]. Typically, this is referred to as depletion in the space charge region, and the opposite effect (space charge accumulation) occurs in p-type materials [49,52]. We note, however, that the space charge is often also associated with surface point defects, where for example oxide vacancies may accumulate on a surface of a metal oxide. Generally, a dynamic equilibrium should be achieved between bound and free charges on the surface determining the space charge features.

The overall increase/decrease in the energy levels of the electrons near a surface is known as the surface band bending effect, and has implicit links to properties such as the ionisation potential of a material [49,52,53]. Of the materials of interest in this study, MgO has been investigated previously in this context: the ionisation potential was calculated using embedded-cluster methods to decrease for the (100) surface when compared to the bulk [29,28], i.e. implying upward bending of the valence band maximum (VBM), which is confirmed by the experiment [54]. Upward bending for the valence band at the surface of MgO slabs has also been reported by Ochs et al., in a comparative study of
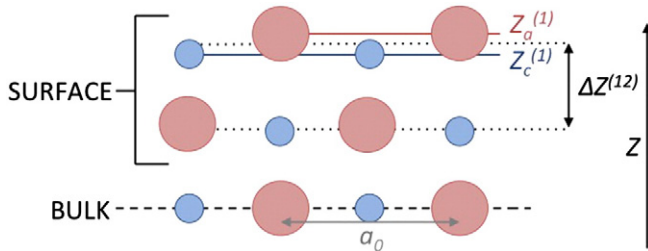
Table 2
Structural properties obtained from previous theoretical and experimental work for the (100) surfaces of the alkaline earth metal oxides CaO, SrO and BaO, along with surface energies (γ_{surf}). Method acronyms are as stated in the text, and the -SIC appenditure on to LDA stands for "self-interaction correction", as applied in these specific calculations. The exchange-correlation functional is given in parentheses for theoretical results.

	Method	[Ref]	d_{rum} (%)	d_{rel} (%)	γ_{surf} (J/m²)
CaO:	LDA (VWN)	[23]	−1.31	−2.25	0.87
	LDA (PZ81)	[41]	−0.6	−2.3	0.81
	LDA-SIC (PZ81)	[43]	−1.1	−2.0	0.95
	GGA (PBE)	[23]	−0.55	−1.69	0.66
	GGA (PBE)	[41]	−0.2	−2.7	0.66
	GGA (PW91)	[44]	−0.68	−1.12	0.63
	GGA (PW91)	[45]	−0.3	−1.8	0.68
	LEED	[48]	2	−1	–
SrO:	LDA (PZ81)	[41]	−1.5	−3.2	0.69
	LDA-SIC (PZ81)	[43]	−2.5	−2.6	0.84
	GGA (PBE)	[41]	−1.3	−3.0	0.61
	GGA (PW91)	[44]	−2.26	−1.67	0.53
	GGA (PW91)	[45]	−2.0	−2.0	0.53
BaO:	LDA (PZ81)	[41]	−1.8	−4.6	0.56
	LDA-SIC (PZ81)	[43]	−5.8	−6.3	0.57
	GGA (PBE)	[41]	−1.6	−4.0	0.42
	GGA (PW91)	[44]	−4.89	−2.45	0.33
	GGA (PW91)	[45]	−3.8	−4.0	0.33

ultraviolet spectroscopy and DFT: the increase in energy of the VBM at the surface was seen, though not quantified, when the calculated density of states (DOS) were decomposed into contributions from each slab layer [55]. Interestingly, however, experimental and computational measurements put the conduction band minimum (CBM) of MgO above the vacuum level [28,56–59], i.e. bulk MgO has a *negative* electron affinity (DFT calculations also produced the same observations for CaO and SrO [59]). However, when the MgO (100) surface was further investigated, a *positive* electron affinity is encountered in the experiment [60], implying downwards band bending. This effect is also seen in computational studies, but the band bending is less pronounced and so a negative electron affinity is still reported [28,61].

In this work, we therefore build on previous studies with a systematic investigation of (100) surfaces using up-to-date GGA and Hybrid-DFT exchange-correlation functionals. We examine the (100) surfaces for rocksalt-structured group 2 metal oxides, namely MgO, CaO, SrO and BaO, calculating structural, energetic and electronic properties. Secondly we focus on the as yet unstudied surface band bending in these materials, which we quantify by examining the density of states for each system as a function of depth from the system surface, and we are able to provide some understanding for the experimental observation of a positive electron affinity at the MgO (100) surface.

2. Methodology

DFT calculations have been performed using a plane-wave basis set, as implemented in the software package VASP [62,63], to obtain accurate information of the electron energy levels. Only the valence electronic configurations were calculated explicitly, with interactions between the core and valence electrons described using the PAW method [64]; the valence electronic configurations for O ($2s^22p^4$), Mg ($2p^63s^2$), Ca ($3s^23p^64s^2$), Sr ($4s^24p^65s^2$) and Ba ($5s^25p^66s^2$) all included semi-core states. A plane-wave kinetic energy cutoff of 500 eV and a Γ-centred Monkhorst-Pack grid [65] across the 1st Brillouin zone have been used throughout, with **k**-points spacing of 0.04 Å^{-1} or denser. In order to create the surface models, we firstly optimised the sole unit cell parameter for cubic rocksalts, a_0, using the analytical stress tensor, as using experimental lattice parameters would result in artificial strain. During the optimisation of a_0 we adjusted the number of plane waves between steps to remove Pulay stress [66]. Structural convergence was achieved when the forces on all atoms were less than 0.01 eV Å^{-1}. We have used the GGA exchange-correlation (XC) functionals PBE [67] and PBESol, the latter being a re-

parameterisation of PBE specifically designed for studying solids [68], as well as their non-local hybrid counterparts, namely PBE0 [69] and PBESol0, wherein 25% of Hartree-Fock exchange is combined with the GGA XC functionals [69,70]. The choice of 25% Hartree-Fock exchange is not only due to the accurate results previously reported using this parameterisation [69,70], but also the unbiased nature (i.e. physical arguments instead of empirical fitting) in which this exact-exchange contribution is decided upon, which is important when studying systems with varying properties [71]. Details of the calculated lattice parameters, and electronic properties for these bulk systems, are provided in our recent publication, and the reader is directed there for a more detailed discussion [59].

To represent surface termination, slab supercells were then constructed from the optimised bulk unit cell with a (100) termination. The electronic structure in the middle of the slab should correctly reproduce the bulk electronic structure, to achieve which, it was necessary to include eight layers (16 atoms) in the slab model and a vacuum layer of at least 18 Å.

For this design, we found that the scatter of the O_{1s} eigenvalues was converged to 0.01 eV at the Γ-point, i.e. bulk-like, before geometry optimisation, and the dipole through a surface after geometry optimisation (as checked using a polarisable forcefield [40]) was converged to 0.0002 e·Å. All parameters for electronic calculations were as used for the bulk calculations, except for the **k**-point mesh where only 1 **k**-point was used in the z-direction, i.e. normal to the surface. Surface energies were obtained by performing calculations on the slab system fixed in the bulk structure and then geometry optimisation was carried out with no atomic constraints and supercell parameters fixed, with structural convergence again achieved when the forces on all atoms were less than 0.01 eV Å^{-1}. The projected density of states (DOS) was extracted separately for each layer of atoms in the slab, and then plotted for analysis, as detailed in our recent publication on the electronic structure of non-polar ZnO surfaces [72].

To describe structural changes after geometry optimisation of the slab model, we use both surface rumpling (d_{rum}) and the change in the first interlayer spacing (d_{rel}), as illustrated in Fig. 1, and defined as in Eqs. (1) and (2), respectively. The cleavage energy (E_{cle}) and the subsequent relaxation energy (E_{rel}) can de defined as [41]:

$$E_{cle} = \frac{E_{slab}^{(unrel)} - NE_{bulk}}{2A}, \tag{3}$$

$$E_{rel} = \frac{E_{slab}^{(relax)} - E_{slab}^{(unrel)}}{2A}, \tag{4}$$

where $E_{slab}^{(unrel)}$ and $E_{slab}^{(relax)}$ is the energy of our slab calculated before and after structural relaxation, E_{bulk} is the energy of the bulk unit cell, N is the number of bulk units in our slab model (= 8), and A is the surface area. A factor of two arises because there are two surfaces in the model — top and bottom. E_{cle} is a positive energy, i.e. unfavourable, whereas E_{rel} is negative, and the energies can then be combined to give the surface energy, $\gamma_{surf} = E_{cle} + E_{rel}$.

Typically in 3D periodic calculations, it is not possible to access the reference "vacuum" potential, and so electronic levels cannot be aligned between calculations. However, for slab models one can obtain the plateau of the electrostatic Hartree potential around the mid-point of the vacuum gap, or the "background potential", V_{bg}, which then serves as a common absolute reference, approximating as the vacuum potential at the limit of infinite slab separation. Aligning a Kohn–Sham eigenvalue (ϵ) relative to vacuum is then achieved via [59,73]:

$$I = -eV_{bg} - \epsilon, \tag{5}$$

where e is the charge of an electron and I is used to represent the ionisation potential, akin to Koopmans' theorem [74]. The validity of Koopmans' theory for Kohn–Sham eigenvalues has been debated previously [75–81]: the method results in significant errors in *absolute*

ionisation potentials for *core* electrons [81,80,78], however it does produce reasonably accurate ionisation potentials for *valence* electrons [76,77], as analysed here, as well as accurately reproducing the *relative* shift in binding energies for *core* electrons in different chemical environments [78]. Calculating the first ionisation potential, which involves taking an electron from the valence band maximum (VBM) to the vacuum, is thus $I_{VBM} = -eV_{bg} - \epsilon_{VBM}$. In our recent work we illustrated how one can also access the eigenstates for bulk environments using slab model calculations, by the explicit compensation of surface polarisation effects [59]. Here, we compare the absolute bulk eigenvalues with the calculated surface levels in this work as a method of quantifying surface band bending.

3. Results

The structural, energetic and electronic properties of the bulk materials are taken from our recent work on the ionisation potential of bulk rocksalt-structured metal oxides [59], where these bulk observables are included in the Supporting information (SI). As these results are well discussed previously, we do not consider them further in the context of this work and instead direct the reader to the highlighted reference and citations therein.

3.1. Structure and energetics

Our calculated structural data for the relaxed (100) surface of MgO, CaO, SrO and BaO are presented in Fig. 2 and Table 3. For MgO, both d_{rum} and d_{rel} are positive in all our calculations, and the difference between the parameterisations of the GGA and the Hybrid counterparts are small, with a range of 0.23% for both structural parameters. Our GGA-based results are in agreement for d_{rum} with the previous PBE and PW91 calculations (2.2–2.4%, Table 1), but not the more recent dispersion corrected PBE-D calculations (0.06%) of Schüller et al. [39]. Furthermore, we calculate d_{rel} as being positive whereas in the previous literature d_{rel} is negative, though it seems that the larger negative values are prominent in relatively thin slab models (4–6 layers) whereas the thicker models of 7, 9 and 11 layers in the work of Skorodumova et al. give $d_{rel} = 0\%$ [44]. Irrespective, the only previous work where $d_{rel} > 0\%$ used the LDA approach, and even that contradicted other reports [23,41–43].

Descending group 2, for CaO we see a similar trend as MgO for d_{rum}, with the PBESol (-0.84%) and PBESol0 (-1.03%) results lower than for PBE and PBE0 (-0.64 and -0.98%, respectively). d_{rel} is also lower for PBESol (-2.32%) than PBE (-1.89%), though the difference is significantly reduced with the introduction of HF contributions (PBE0: -1.41%; PBESol0: -1.49%). Comparing our CaO results to those in Table 2, we notice a greater similarity to previous work than for MgO,

Table 3

DFT calculated d_{rum} and d_{rel} for the relaxed (100) surfaces of the alkaline earth metal oxides MgO, CaO, SrO and BaO, along with surface energies (γ_{surf}). The PBE XC functionals are given in italic (GGA and Hybrid-counterpart), whilst the PBESol XC functionals are given in bold.

	Method	d_{rum} (%)	d_{rel} (%)	γ_{surf} (J/m^2)
MgO:	*PBE*	*2.31*	*0.20*	*0.92*
	PBESol	**2.20**	**0.34**	**1.02**
	PBE0	*2.22*	*0.11*	*1.03*
	PBESol0	**2.08**	**0.19**	**1.11**
CaO:	*PBE*	-0.64	-1.89	*0.74*
	PBESol	**-0.84**	**-2.32**	**0.79**
	PBE0	-0.98	-1.41	*0.73*
	PBESol0	**-1.03**	**-1.49**	**0.80**
SrO:	*PBE*	-2.15	-2.43	*0.60*
	PBESol	**-2.40**	**-3.32**	**0.63**
	PBE0	-2.18	-2.63	*0.63*
	PBESol0	**-2.34**	**-2.49**	**0.64**
BaO:	*PBE*	-4.94	-5.66	*0.34*
	PBESol	**-5.70**	**-5.76**	**0.37**
	PBE0	-4.74	-4.98	*0.38*
	PBESol0	**-4.91**	**-5.26**	**0.43**

with d_{rum} and d_{rel} negative in all cases; our calculated structural properties fall within the range of previous results. It is notable that again d_{rum} from Hybrid-DFT is lower than previous GGA calculations, and close to the LDA results, but that this is not the case for d_{rel}. We note that the negative value of d_{rum} that we have calculated for CaO, which implies that the cations protrude above the anions at the surface, is not expected if one considers simply the ionic radii of the elements: Ca^{2+} (1.14 Å) is smaller than O^{2-} (1.26 Å) [82], and so one would expect the larger O^{2-} anions to protrude above the Ca^{2+} cations. However, $d_{rum} < 0\%$ for both our results and the previous work (Table 2), which highlights the influence of other properties, such as atomic polarisability, on the surface structure of these binary oxides.

A significant difference is encountered for SrO and BaO, as the Hybrid-DFT calculations do not necessarily lower d_{rum} and d_{rel}. Starting with CaO, d_{rum} for PBE (-2.15%) is higher than PBE0 (-2.18%), however the inverse is seen for PBESol (-2.40%) and PBESol0 (-2.34%) and the same trends are more pronounced for d_{rel}. For BaO, all Hybrid-DFT results are higher than the GGA counterparts: d_{rel} for PBE (-5.66%) is almost 0.7% higher for PBE0 (-4.98%), and there are similar differences of 0.5% between PBESol (-5.76%) and PBESol0 (-5.26%).

When compared to the previous work, our PBE results for SrO are within the range of previous GGA calculations. However for PBESol, we find that d_{rum} and d_{rel} are lower than this previous GGA work, by up to 0.32% for d_{rel}. We add that for our SrO Hybrid-DFT calculations, the results also fall within the range of previous results and the same
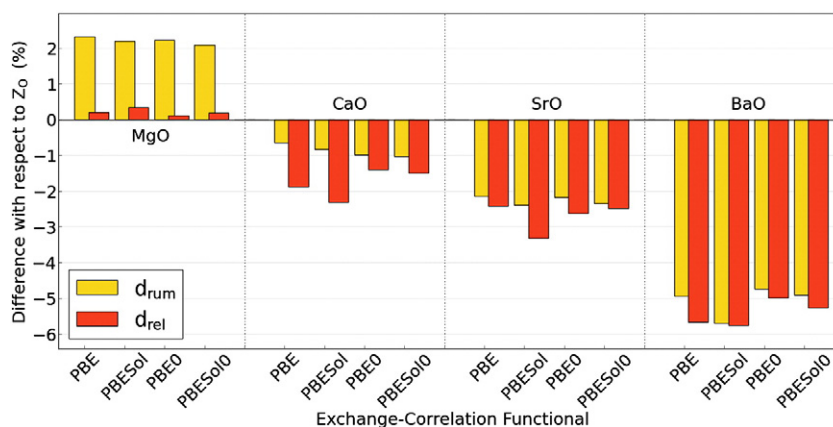

Fig. 2. Rumpling (d_{rum}) and surface relaxation (d_{rel}) of the relaxed (100) surfaces, as a function of the exchange-correlation functionals used: PBE, PBESol, PBE0 and PBESol0. Each set of results is grouped together by system, namely MgO, CaO, SrO and BaO (left to right).

applies for BaO, though the range is much greater for the latter. For BaO, Skorodumova et al. provide the most reliable GGA results [44], due to their thick slab models, and their calculated d_{rum} of -4.89% matches our PBE (-4.94%) calculations but not the PBESol (-5.70%), with a difference of 0.8% meaning our result is closest to the LDA-SIC calculations (-5.8%) of Baumeier et al. [43]; for d_{rel} both our PBE and PBESol values are also closest to these LDA-SIC results (-6.3%).

Also reported in Table 3 are γ_{surf} from our calculations. γ_{surf} is dominated by E_{cle}, with relaxation contributing energies of 0.01 J/m^2 $< E_{rel} < 0.07$ J/m^2. The minimum (CaO) and maximum (BaO) of E_{rel} correlate strongly with the absolute magnitude of d_{rum} for these systems. Overall, γ_{surf} was found to increase in Hybrid-DFT calculations, compared to GGA, but only by at most 0.11 J/m^2. LDA and GGA binding energies are commonly underestimates, due to the inability of these XC functionals to deal with the self-interaction [83,84]. However, we note that in fact PBESol gives results very similar to PBE0, making this an affordable way to calculate desirable structural and energetic properties at the GGA level. In general, we find that γ_{surf} for PBE, PBESol, PBE0 and PBESol0 is greater than most previous GGA results, though lower than the LDA results. We note that for MgO there is reasonable agreement between the experiment (1.04 J/m^2, [46]) and calculations using PBESol (1.02 J/m^2) and PBE0 (1.03 J/m^2).

3.2. Electronic properties

In Table 4 we present the surface-dependent (^{s}) first ionisation potential (I^s_{VBM}) for the (100) surfaces of MgO, CaO, SrO and BaO, along with previously published bulk (^{b}) ionisation potentials (I^b_{VBM}) [59]. I^s_{VBM} is calculated in a manner analogous to I in Eq. (5):

$$I^s_{VBM} = -eV_{bg} - \epsilon^s_{VBM}. \qquad (6)$$

For MgO, CaO and SrO we find that there is a significant reduction in I^s_{VBM} compared to the bulk. This reduction in I^s_{VBM} marginally increases for the GGA calculations, from 0.53 to 0.69 eV, as we progress from MgO to SrO, but the trend is not as clearly shown by our Hybrid-DFT calculations, with the reduction in I^s_{VBM} ranging from 0.37 eV (MgO/PBE0) up to 0.58 eV (CaO/PBESol0). Most interesting are the results for BaO, where significantly different behaviour is observed: the reduction in I^s_{VBM} for GGA calculations is ~0.2 eV, but for Hybrid-DFT we see an *increase* in I^s_{VBM}, of 0.04 and 0.08 eV for PBE0 and PBESol0, respectively, implying that in fact we have a slight downward shift of the background potential in the slab and/or downwards band bending in the VBM.

Overall, however, our results show changes in I^s_{VBM} at surfaces, other than BaO, meaning significant reduction in energy for the valence electrons that implies upward band bending, which has not been reported previously. We add that for MgO our results match the previous work of Sushko et al. where the MgO (100) surface ionisation potential was calculated as ~6.5 eV using a Hybrid-DFT embedded-cluster model [28].

Upwards and downwards band bending are prevalent in n- and p-type materials [85,27,52,49], respectively, though recent work has shown that the magnitude of band bending is not necessarily equal for both the valence and conduction band edges [86–88]. In the case of a two-sided slab model, charge accumulation towards or away from the slab surfaces also creates symmetric surface dipoles; and geometry changes sustained during structural optimisation, such as surface rumpling, lead to the formation of ionic dipoles/quadrupoles that also alter the electrostatic potential of the slab. As a result, this charge redistribution creates a voltage offset akin to the planar parallel-plate capacitor model [59,89]. As a specific example, a negative charge accumulation in the middle of a slab system would result in a dipole forming on either side that points out the surface, which would raise the potential in the slab and, thus, the energy of the electronic states, in turn lowering I^s_{VBM}. For the systems presented, analysis of charge transfer using the Bader method [90] shows that, despite their lower coordination, the net charge of the surface atoms is identical to equivalent species in the middle of the slab (to 2 decimal places). This means that there is no charge transfer between surface and bulk atoms, however this does not account for polarisation of the electrons around each nucleus i.e. atomic polarisability.

Clearly, therefore, the formation of surface dipoles needs a more detailed analysis. To isolate the multipolar contributions to band bending we calculated the projected density of states for each layer of the slab in each calculation, focusing on the shift in energy for specific states as one approaches the surface from the bulk. We present in Table 5 the effective band bending for the valence and conduction band (ΔVB and ΔCB, respectively) by noting the change in band energies between bulk(-like) and surface layers in the plane-projected DOS. We add that $\Delta E_g = \Delta$CB $- \Delta$VB < 0 eV is equivalent to a reduction of the band gap (E_g) at the surface of the material. Additionally, by assuming that all surface-induced changes to I^b_{VBM}, resulting in I^s_{VBM}, are due to either: bending of the valence band at the surface (ΔVB); or multipolar effects shifting the background potential (D_s); then the change in the ionisation potential can be defined as $\Delta I_{VBM} = \Delta$VB $+ eD_s$, where e is the electron

Table 4
DFT calculated I^s_{VBM} for the (100) surfaces of the alkaline metal oxides MgO, CaO, SrO and BaO, for each XC functional. The difference between the I^s_{VBM} and the bulk ionisation potential (I^b_{VBM}) denoted as ΔI_{VBM}, is also presented. I^b_{VBM} values were calculated using a polarisation-corrected slab approach and are presented with the bulk band-gap (E_g), both as calculated in our previous work [59]. The PBE XC functionals are given in italics (GGA and Hybrid-counterpart) whilst the PBESol XC functionals are given in bold.

	Method	I^s_{VBM} (eV)	I^b_{VBM} (eV)	ΔI_{VBM} (eV)	E_g (eV)
MgO:	*PBE*	*5.22*	*5.75*	*0.53*	*4.45*
	PBESol	**5.26**	**5.81**	**0.55**	**4.61**
	PBE0	*6.52*	*6.89*	*0.37*	*7.24*
	PBESol0	**6.57**	**6.97**	**0.40**	**7.38**
CaO:	*PBE*	*4.01*	*4.67*	*0.66*	*3.63*
	PBESol	**4.12**	**4.74**	**0.62**	**3.52**
	PBE0	*5.26*	*5.64*	*0.38*	*6.04*
	PBESol0	**5.32**	**5.90**	**0.58**	**5.94**
SrO:	*PBE*	*3.53*	*4.22*	*0.69*	*3.27*
	PBESol	**3.62**	**4.31**	**0.69**	**3.75**
	PBE0	*4.73*	*5.21*	*0.48*	*5.47*
	PBESol0	**4.82**	**5.30**	**0.48**	**5.37**
BaO:	*PBE*	*3.14*	*3.37*	*0.23*	*3.27*
	PBESol	**3.12**	**3.32**	**0.20**	**3.29**
	PBE0	*4.18*	*4.14*	*−0.04*	*4.01*
	PBESol0	**4.25**	**4.17**	**−0.08**	**3.84**

Table 5
DFT calculated ΔVB and ΔCB for the relaxed (100) surfaces of the alkaline metal oxides MgO, CaO, SrO and BaO, along with the deduced change in band gap (ΔE_g) and the dipolar shift in the background potential (D_s). The PBE XC functionals are given in italics (GGA and Hybrid-counterpart), whilst the PBESol XC functionals are given in bold. An MgO/PBE calculation with a double-thickness 16-layer slab gave results for I^s_{VBM}, ΔVB and D_s that vary from the 8-layer slab by -0.02 eV, -0.05 eV and $+0.08$ V, and these differences should be regarded as the error bars on our results.

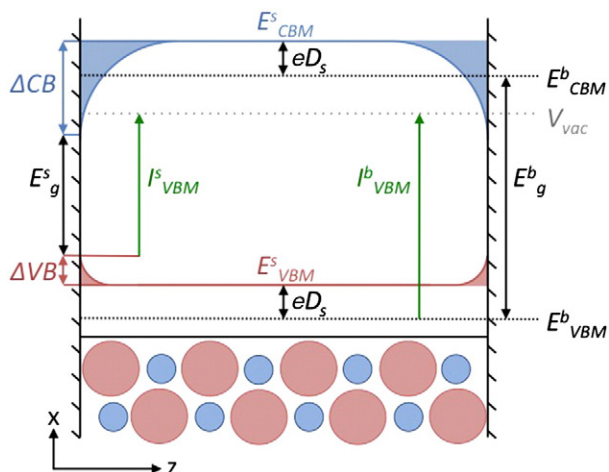|	Method	ΔVB (eV)	ΔCB (eV)	ΔE_g (eV)	D_s (V)
MgO:	*PBE*	*−0.28*	*−1.22*	*−0.94*	*0.81*
	PBESol	**0.03**	**−1.22**	**−1.25**	**0.52**
	PBE0	*−0.33*	*−1.87*	*−1.54*	*0.70*
	PBESol0	**0.00**	**−1.92**	**−1.92**	**0.40**
CaO:	*PBE*	*0.18*	*−0.51*	*−0.69*	*0.48*
	PBESol	**0.39**	**−0.17**	**−0.56**	**0.23**
	PBE0	*0.26*	*−0.88*	*−1.04*	*0.12*
	PBESol0	**0.14**	**−0.86**	**−1.00**	**0.58**
SrO:	*PBE*	*0.14*	*−0.58*	*−0.72*	*0.55*
	PBESol	**0.16**	**−0.24**	**−0.40**	**0.53**
	PBE0	*0.19*	*−0.69*	*−0.88*	*0.29*
	PBESol0	**0.30**	**−1.02**	**−1.32**	**0.18**
BaO:	*PBE*	*0.11*	*0.13*	*0.02*	*0.12*
	PBESol	**−0.02**	**0.24**	**0.26**	**0.22**
	PBE0	*0.02*	*−0.15*	*−0.13*	*−0.06*
	PBESol0	**0.00**	**0.00**	**0.00**	**−0.08**

Fig. 3. Schematic representation of a slab of MgO, and the consequential band bending effects due to the presence of a surface. O^{2-} anions and Mg^{2+} cations are represented by red and blue spheres, respectively. The same colour scheme is used to represent the valence (red) and conduction (blue) band minima/maxima (E^s_{VBM} and E^s_{CBM}, respectively), as they are positioned on these O^{2-} anions and Mg^{2+} cations, respectively. We illustrate the change in the VB and CB as one approaches the slab surface, ΔVB and ΔCB, as well as the electrostatic dipolar shift (eD_s) in the VBM and CBM positions with respect to the bulk, where the bulk VB and CB are shown with black dotted lines as E^b_{VBM} and E^b_{CBM}. The band gap at the surface (E^s_g) shrinks considerably compared to the bulk (E^b_g), by up to 2.56 eV in the case of PBE0. Finally, the universal vacuum level (V_{vac}) is presented in grey, against which we are able to align the VB edges by calculating the ionisation potential in the slab and bulk systems, labelled in green as I^s_{VBM} and I^b_{VBM}, respectively.

charge, and thus we can deduce D_s from our results as illustrated in Fig. 3.

It is immediately noticeable for MgO that there is very little change in the VB edge at the slab surface, with ΔVB either ~ -0.3 or 0.0 eV for PBE- and PBESol-based XC functionals, respectively. This result implies a slight downward bend in the VBM for PBE and PBE0, which does not correlate with the previous observation that I^s_{VBM} for MgO tends to be slightly smaller than I^b_{VBM} [28,91] until one considers the influence also of D_s, as discussed below. However, more prominent for the band positions is the significant downward bending of the conduction band, with ΔCB ranging between -0.94 (PBE) and -1.92 (PBESol0) eV. This downward bending can be attributed to the reduced coordination of the surface cations, which leads to an increase in the electrostatic potential at these sites [61], and as a consequence, the CB is bent *below* the vacuum level in the Hybrid-DFT calculations (for GGA-calculations it was already positioned below the vacuum level; see Table 4). Previous Hybrid-DFT embedded-cluster calculations found an increase in the electron affinity for the MgO (100) surface with reducing cation coordination [28,61], but Sushko et al. reported that these results still placed the CBM in their calculations for a pristine surface *above* the vacuum level – i.e. a negative electron affinity – whereas experiments show that the CBM is *below* the vacuum level [60], with an electron affinity of ~1 eV. Sushko et al. comment that their results may be incorrect arising from quantum confinement [28], due to the finite size of the embedded-cluster, and from this perspective our plane-wave results perhaps give greater insight into the experimental observations, as we calculate the CBM as being *below* the vacuum level using Hybrid-DFT, by 0.82 (PBE0) and 1.11 eV (PBESol0), with the two-sided slab model.

We note at this point that there is no discussion of the cleanliness of the MgO surface in the experimental work of Stevenson and Hensley [60], which is not ideal given that properties like the electron affinity may depend on the surface structure. We consider that surface defects, such as oxygen vacancies, will not be influential on these properties in MgO, as the defect states will be counterbalanced by cation vacancies

or charge acceptors (e.g. Li) and thus the effects limited to local areas. Furthermore, if such defects were to aggregate at the surface then we should expect uniform band-bending; however this has not been seen in experiment nor in our calculations. There remains, however, a possibility that the effect is enhanced by e.g. surface stepping, where significant change in morphology results in a large proportion of surface sites to be even more under-coordinated. By the nature of this surface, the number of differently coordinated sites in both anion and cation sublattices would be equal (neglecting point defects). Therefore, we need more experimental work to explore this area further.

The observed downward bending of the CBM in MgO is also apparent for CaO and SrO. In all cases, it is greater for Hybrid-DFT than for GGA calculations, and is greatest for PBE0. In fact, for all 3 materials PBE0 and PBESol0 position the CB below the vacuum level at the slab surface: for CaO, the slab CBM is calculated as 0.36 and 0.24 eV, using PBE0 and PBESol0 respectively, whilst for SrO the slab CBM is calculated as 0.14 and 0.77 eV using the same XC functionals. In the bulk the inverse is found, as can be deduced from Table 4, i.e. the bulk materials have a negative electron affinity [59]: in the GGA calculations, the bulk CBM is below the vacuum level due to the underestimation of the system band gap (Table 4). Furthermore, ΔCB is always negative in these calculations, ranging from -1.22 eV for MgO up to -0.17 eV for CaO when using PBESol, and so the CBM is lower in energy at the surfaces than for the bulk due to the band bending. In contrast, ΔVB is positive for CaO and SrO, indicating upward band bending, but only in the range $0.14 < \Delta$VB < 0.39 eV and so the effects on properties such as I^s_{VBM} are limited. However, combining ΔVB with ΔCB results in an overall reduction of the bandgap (ΔE_g) up to as much as 1.92 eV for MgO when using PBESol0, which could have significant effects on the material properties at the surface. Finally, for MgO, CaO and SrO, D_s is appreciable, with values in the range $0.12 < D_s < 0.81$ V implying that I^s_{VBM} is reduced partly by the formation of a surface-induced electronic dipole, when compared to I^b_{VBM}.

The results are different for BaO: ΔVB is similar to the other oxide materials investigated, with $-0.02 < \Delta$VB<0.11 eV meaning a slight upward band bending, which can be attributed to the undercoordination of the surface anions leading to reduced electrostatic potentials in these regions. However, ΔCB is now considerably reduced on comparison to the other materials investigated, with values ranging through both negative (PBE0: -0.15 eV) and positive (PBESol: 0.24 eV); the former is the only example for BaO that we discover of downwards band bending in the CB, though it is worth noting that, for all materials, ΔCB is always highest (i.e. most positive) when using the PBESol XC functional and so for BaO this exceptional positive value may be an artefact of the functional itself. Such small band bending results in relatively little change in E_g overall, with $-0.13 < \Delta E_g < 0.26$ eV, and consequently D_s is smaller than seen for MgO, CaO and SrO.

4. Summary and conclusions

We have calculated structural and electronic properties for the rocksalt oxide structures formed by the Group 2 alkaline earth metals using density functional theory with a range of exchange-correlation functionals. It is found that MgO favours a surface rumpling arrangement where the oxygen anion protrudes farther from the surface than the magnesium cations by up to 2.31%. In the cases of CaO, SrO and BaO, however, the inverse is true with the cations protruding farther as one descends the group to heavier elements, up to 5.70% for BaO with some Hybrid-DFT functionals.

Surface relaxations follow a similar trend as one descends the periodic table, with decreasing distances between the surface and sub-surface layers. MgO is the only system where we see an expansion between the surface layers, and for all other systems contraction is prominent, with values of -5.76% calculated for BaO using PBESol. In general, the contraction of the interlayer distance is greater than the surface rumpling, though the two appear to be closely linked.

Electronic properties calculated included the surface ionisation potential and band bending. In general, the surface ionisation potentials for MgO, CaO and SrO are smaller than in our previous bulk calculations, with the results for MgO matching previously calculated results of ~6.5 eV for the (100) surface. This decreased ionisation potential implies significant upward band bending of ~0.5 eV in the valence band at the surface.

More detailed analysis of the band bending was conducted via decomposition of the density of states into layer-by-layer contributions, where multiple factors were found to affect the changes in ionisation potential. The change in the valence band maxima are limited to a range between − 0.33 and 0.39 eV, which is much less than the change in the ionisation potentials between the bulk and surface. We explain that the other contribution to the ionisation potential changes are the effect of a voltage offset encountered due to the formation of a surface dipole in the slab, the magnitude of which is similar for MgO, CaO and SrO; for BaO the voltage offset is minimal.

Finally, we also analyse the bending of the conduction band and observe that this shifts downwards, i.e. in the opposite direction from the valence band, in almost all cases. This effect is significant, with changes of up to 1.92 eV for MgO/PBESol0, and consequently results in band-gap closure for these materials at the (100) surface. Furthermore, the downwards bending of the conduction band minimum brings this band edge *below* the vacuum level, unlike previous calculations, which results in a positive electron affinity for the MgO surface; this corroborates previous experimental work where an electron affinity of ~1 eV was reported. However, further work is required to verify that other structural factors, such as undercoordinated step sites, are not affecting significantly these properties.

In the future, we will expand our analysis to include higher energy terminations and hope to use these observations in summarising the effects for other commercially important materials such as CdO and SrTiO$_3$, which have been specifically shown to form 2D electron gases at their surfaces [86,92].

Acknowledgements

References

[1] K. Honkala, Surf. Sci. Rep. 69 (4) (2014) 366.
[2] H. Hattori, Appl. Catal. A Gen. 222 (1–2) (2001) 247.
[3] J. Goniakowski, C. Noguera, Surf. Sci. 340 (3) (1995) 191.
[4] G. Pacchioni, H. Freund, Chem. Rev. 113 (6) (2013) 4035.
[5] H.A. Al-Abadleh, V.H. Grassian, Surf. Sci. Rep. 52 (3–4) (2003) 63.
[6] V.E. Henrich, P.A. Cox, The Surface Science of Metal Oxides, vol. 1, Cambridge University Press, Cambridge, UK, 1996.
[7] D.P. Woodruff, Chem. Rev. 113 (6) (2013) 3863.
[8] C. Noguera, Physics and Chemistry at Oxide Surfaces, Cambridge University Press, 1996.
[9] P. Liu, T. Kendelewicz, G.E. Brown Jr., G.A. Parks, Surf. Sci. 412–413 (1998) 287.
[10] P. Liu, T. Kendelewicz, G.E. Brown, G.A. Parks, P. Pianetta, Surf. Sci. 416 (1-2) (1998) 326.
[11] P. Liu, T. Kendelewicz, G.E. Brown Jr., Surf. Sci. 412 (1998) 315.
[12] W. Langel, M. Parrinello, Phys. Rev. Lett. 73 (1994) 504.
[13] C.A. Scamehorn, N.M. Harrison, M.I. McCarthy, J. Chem. Phys. 101 (2) (1994) 1547.
[14] K. Refson, R.A. Wogelius, D.G. Fraser, M.C. Payne, M.H. Lee, V. Milman, Phys. Rev. B 52 (1995) 10823.
[15] W. Langel, M. Parrinello, J. Chem. Phys. 103 (8) (1995) 3240.
[16] J. Carrasco, F. Illas, N. Lopez, Phys. Rev. Lett. 100 (2008) 016101.
[17] H. Grönbeck, I. Panas, Phys. Rev. B 77 (2008) 245419.
[18] T. Seki, K. Akutsu, H. Hattori, Chem. Commun. (2001) 1000.
[19] T. Seki, H. Hattori, Chem. Commun. (2001) 2510.
[20] M. Calatayud, A.M. Ruppert, B.M. Weckhuysen, Chem. Eur. J. 15 (41) (2009) 10864.
[21] M. Calatayud, Catal. Today 152 (1–4) (2010) 88.
[22] E.J.W. Verwey, Recl. Trav. Chim. Pays-Bas 65 (7) (1946) 521.
[23] D.R. Alfonso, J.A. Snyder, J.E. Jaffe, A.C. Hess, M. Gutowski, Phys. Rev. B 62 (2000) 8318.
[24] G.W. Watson, E.T. Kesley, N.H. de Leeuw, D.J. Harris, S.C. Parker, J. Chem. Soc. Faraday Trans. 92 (3) (1996) 433.
[25] D.E. Deacon-Smith, D.O. Scanlon, C.R.A. Catlow, A.A. Sokol, S.M. Woodley, Adv. Mater. 26 (42) (2014) 7252.
[26] F.W. de Wette, W. Kress, U. Schröder, Phys. Rev. B 32 (1985) 4143.
[27] W. Mönch, Semiconductor Surfaces and Interfaces, vol. 26, Springer, 2001.
[28] P.V. Sushko, A.L. Shluger, C.A. Catlow, Surf. Sci. 450 (3) (2000) 153.
[29] A.L. Shluger, P.V. Sushko, L.N. Kantorovich, Phys. Rev. B 59 (1999) 2417.
[30] P.V. Sushko, J.L. Gavartin, A.L. Shluger, J. Phys. Chem. B 106 (9) (2002) 2269.
[31] C.G. Kinniburgh, J. Phys. C Solid State 8 (15) (1975) 2382.
[32] T. Urano, T. Kanaji, M. Kaburagi, Surf. Sci. 134 (1) (1983) 109.
[33] M. Welton-Cook, W. Berndt, J. Phys. C Solid State 15 (27) (1982) 5691.
[34] D. Blanchard, D. Lessor, J. LaFemina, D. Baer, W. Ford, T. Guo, J. Vac. Sci. Technol. A 9 (3) (1991) 1814.
[35] D. Ferry, J. Suzanne, V. Panella, A. Barbieri, M. Van Hove, J.-P. Bibérian, J. Vac. Sci. Technol. A 16 (4) (1998) 2261.
[36] H. Nakamatsu, A. Sudo, S. Kawai, Surf. Sci. 194 (1) (1988) 265.
[37] J. Zhou, H. Lu, T. Gustafsson, P. Häberle, Surf. Sci. 302 (3) (1994) 350.
[38] O. Robach, G. Renaud, A. Barbier, Surf. Sci. 401 (2) (1998) 227.
[39] A. Schüller, D. Blauth, J. Seifert, M. Busch, H. Winter, K. Gärtner, R. Wlodarczyk, J. Sauer, M. Sierka, Surf. Sci. 606 (3) (2012) 161.
[40] G.V. Lewis, C.R.A. Catlow, J. Phys. C Solid State 18 (6) (1985) 1149.
[41] P. Broqvist, H. Grönbeck, I. Panas, Surf. Sci. 554 (2-3) (2004) 262.
[42] C. Quintanar, R. Caballero, V. Castano, Int. J. Quantum Chem. 102 (5) (2005) 820.
[43] B. Baumeier, P. Krüger, J. Pollmann, Phys. Rev. B 76 (2007) 205404.
[44] N.V. Skorodumova, K. Hermansson, B. Johansson, Phys. Rev. B 72 (2005) 125414.
[45] C. Cárdenas, F. De Proft, E. Chamorro, P. Fuentealba, P. Geerlings, J. Chem. Phys. 128 (3) (2008).
[46] G. Jura, C.W. Garland, J. Am. Chem. Soc. 74 (23) (1952) 6033.
[47] Y. Xu, J. Li, Y. Zhang, W. Chen, Surf. Sci. 525 (1) (2003) 13.
[48] M. Prutton, J.A. Ramsey, J.A. Walker, M.R. Welton-Cook, J. Phys. C Solid State 12 (23) (1979) 5271.
[49] Z. Zhang, J.T. Yates Jr., Chem. Rev. 112 (10) (2012) 5520.
[50] R.K. Swank, Phys. Rev. 153 (1967) 844.
[51] K. Jacobi, G. Zwicker, A. Gutmann, Surf. Sci. 141 (1) (1984) 109.
[52] L.J. Brillson, Surfaces and Interfaces of Electronic Materials, Wiley-VCH Verlag, 2010.
[53] H. Lüth, Solid surfaces, interfaces and thin films, vol. 5, Springer, US, 2010.
[54] L.N. Kantorovich, A.L. Shluger, P.V. Sushko, J. Gunster, P. Stracke, D.W. Goodman, V. Kempter, Faraday Discuss. 114 (1999) 173.
[55] D. Ochs, W. Maus-Friedrichs, M. Brause, J. Günster, V. Kempter, V. Puchin, A. Shluger, L. Kantorovich, Surf. Sci. 365 (2) (1996) 557.
[56] R. Whited, C.J. Flaten, W.C. Walker, Solid State Commun. 13 (11) (1973) 1903.
[57] P.D. Johnson, Phys. Rev. 94 (1954) 845.
[58] T. Jaouen, G. Jézéquel, G. Delhaye, B. Lépine, P. Turban, P. Schieffer, Appl. Phys. Lett. 97 (23) (2010) 232104.
[59] A.J. Logsdail, D.O. Scanlon, C.R.A. Catlow, A.A. Sokol, Phys. Rev. B 90 (15) (2014) 155106.
[60] J.R. Stevenson, E.B. Hensley, J. Appl. Phys. 32 (2) (1961) 166.
[61] D. Ricci, G. Pacchioni, P.V. Sushko, A.L. Shluger, J. Chem. Phys. 117 (6) (2002) 2844.
[62] G. Kresse, J. Furthmüller, Comput. Mater. Sci. 6 (1) (1996) 15.
[63] G. Kresse, D. Joubert, Phys. Rev. B 59 (1999) 1758.
[64] P.E. Blöchl, Phys. Rev. B 50 (24) (1994) 17953.
[65] H.J. Monkhorst, J.D. Pack, Phys. Rev. B 13 (1976) 5188.
[66] G.P. Francis, M.C. Payne, J. Phys. Condens. Matter 2 (19) (1990) 4395.
[67] J.P. Perdew, K. Burke, M. Ernzerhof, Phys. Rev. Lett. 77 (18) (1996) 3865.
[68] J.P. Perdew, A. Ruzsinszky, G.I. Csonka, O.A. Vydrov, G.E. Scuseria, L.A. Constantin, X. Zhou, K. Burke, Phys. Rev. Lett. 100 (2008) 136406.
[69] C. Adamo, V. Barone, J. Chem. Phys. 110 (13) (1999) 6158.
[70] M. Marsman, J. Paier, A. Stroppa, G. Kresse, J. Phys. Condens. Matter 20 (6) (2008) 064201.
[71] J.P. Perdew, M. Ernzerhof, K. Burke, J. Chem. Phys. 105 (22) (1996) 9982.
[72] D. Mora-Fonz, J. Buckeridge, A.J. Logsdail, D.O. Scanlon, A.A. Sokol, S.M. Woodley, C.R.A. Catlow, J. Phys. Chem. C 119 (21) (2015) 11598.
[73] A. Walsh, K.T. Butler, Acc. Chem. Res. 47 (2) (2014) 364.
[74] T. Koopmans, Physica 1 (1–6) (1934) 104.
[75] R.S. Mulliken, The theory of molecular orbitals, J. Chim. Phys. 46 (497) (1949).
[76] D.P. Chong, O.V. Gritsenko, E.J. Baerends, J. Chem. Phys. 116 (5) (2002) 1760.
[77] O.V. Gritsenko, B. Braïda, E.J. Baerends, J. Chem. Phys. 119 (4) (2003) 1937.
[78] N.P. Bellafont, F. Illas, P.S. Bagus, Phys. Chem. Chem. Phys. 17 (2015) 4015.
[79] D.J. Tozer, F. De Proft, J. Phys. Chem. A 109 (39) (2005) 8923.
[80] P.S. Bagus, E.S. Ilton, C.J. Nelin, Surf. Sci. Rep. 68 (2) (2013) 273.
[81] P.S. Bagus, Phys. Rev. 139 (1965) A619.
[82] R.D. Shannon, Acta Crystallogr. 32 (5) (1976) 751.
[83] J.P. Perdew, A. Zunger, Phys. Rev. B 23 (1981) 5048.

[84] R.G. Parr, W. Yang, Density Functional Theory of Atoms and Molecules, Oxford, New York, 1989.
[85] A.J. Nozik, R. Memming, J. Phys. Chem. 100 (31) (1996) 13061.
[86] P.D.C. King, T.D. Veal, C.F. McConville, J. Zúñiga Pérez, V. Muñoz Sanjosé, M. Hopkinson, E.D.L. Rienks, M.F. Jensen, P. Hofmann, Phys. Rev. Lett. 104 (2010) 256803.
[87] P.D.C. King, T.D. Veal, C.F. McConville, Phys. Rev. B 77 (12) (2008) 125305.
[88] P.D.C. King, T.D. Veal, P.H. Jefferson, C.F. McConville, H. Lu, W.J. Schaff, Phys. Rev. B 75 (2007) 115312.

[89] K.T. Butler, A. Walsh, Thin Solid Films 559 (2014) 64.
[90] W. Tang, E. Sanville, G. Henkelman, J. Phys. Comput. Mater. 21 (2009) 084204.
[91] K. Yoshino, Y. Morita, T. Nagatomi, M. Terauchi, T. Tsujita, Y. Doi, T. Nakayama, Y. Yamauchi, M. Nishitani, M. Kitagawa, Y. Yamauchi, Y. Takai, Appl. Surf. Sci. 259 (2012) 135.
[92] W. Meevasana, P.D.C. King, R.H. He, S.K. Mo, M. Hashimoto, A. Tamai, P. Songsiriritthigul, F. Baumberger, Z.X. Shen, Nat. Mater. 10 (2) (2011) 114.